RADC-TDR-63-83

January 1963

THIRD QUARTERLY PROGRESS REPORT ON SOLID-STATE CIRCUITS

by

S. Hamilton, W. W. Heinz, S. Okwit,
E. W. Sard, and K. Siegel

AIRBORNE INSTRUMENTS LABORATORY
A DIVISION OF CUTLER-HAMMER, INC.
Deer Park, Long Island, New York

REPORT NO. 1654-I-3
Contract AF 30(602)-2699

Prepared for

Rome Air Development Center
Research and Technology Division
Air Force Systems Command
United States Air Force

Griffiss Air Force Base
New York

NOTICES

Qualified requesters may obtain copies from ASTIA. Orders will be expedited if placed through the librarian or other person designated to request documents from ASTIA.

When U. S. Government drawings, specifications, or other data are used for any purpose other than definitely related Government procurement operation, the Government thereby incurs no responsibility nor any obligation whatsoever; and the fact that the Government may have furnished said drawings, specifications, or other data is not to be regarded by implication or otherwise, as in any manner licensing the holder or any other person or corporation, or conveying any rights or permission to manufacture, use, or sell any patented invention that may in any way be related thereto.

Do not return this copy. Retain or destroy.

RADC-TDR-63-83 January 1963

THIRD QUARTERLY PROGRESS REPORT ON SOLID-STATE CIRCUITS

by

S. Hamilton, W. W. Heinz, S. Okwit,
E. W. Sard, and K. Siegel

AIRBORNE INSTRUMENTS LABORATORY
A DIVISION OF CUTLER-HAMMER, INC.
Deer Park, Long Island, New York

REPORT NO. 1654-I-3
Contract AF 30(602)-2699

Project No. 4506
Task No. 450602

Prepared for

Rome Air Development Center
Research and Technology Division
Air Force Systems Command
United States Air Force

Griffiss Air Force Base
New York

Title of Report

RADC-TDR-63-83

PUBLICATION REVIEW

This report has been reviewed and is approved.

Approved:

ARTHUR J. FROHLICH
Chief, Techniques Laboratory
Directorate of Aerospace Surveillance & Control

Approved:

WILLIAM T. POPE
Acting Director
Director of Aerospace
Surveillance & Control

ABSTRACT

Measurements of linewidth and anisotropy were made on a 600 $4\pi M_s$ Ga-YIG single-crystal ferrite. The linewidth behaved normally with respect to its variation with crystal axis orientation; that is, the linewidths were maximum (7.8 oersteds) with the external fields along the easy axis and minimum (3.7 oersteds) along the hard axis. Measurements on the decline of the susceptibility yielded critical threshold levels that agree well with the values predicted from the measured linewidths. It is expected that limiting levels in the region of -20 dbm should be realizable in the UHF region with this material.

A low-threshold varactor limiter was designed and constructed using a varactor-loaded single-tuned circuit. By using the field build-up characteristic of a highly regenerative circuit, threshold-limiting levels of less than -20 dbm were achieved. This technique yields a narrow-band device in which bandwidth is traded for limiting level. The limiter had a dynamic range of greater than 40 db, an insertion loss of 1.8 db, and a bandwidth of 2 Mc. Cascading the limiter with the high-power broad-band limiter, developed earlier on this project (described in a previous quarterly progress report), yields an ultra-dynamic range of 70 db, and an overall insertion loss of 2 db while still maintaining its low threshold level.

Investigations of the performance of commercially available three-port C-band circulators, relative to the theoretical performance expected from Bosma's analysis, was continued. Modifications of Bosma's equations were made to allow for negative μ_{eff} values and extended frequency vari-

ation. The effect of imperfectly matching a circulator, by the technique derived earlier in the project, was analyzed. In addition, modifications of a Bendix circulator incorporating a double-tuned matching network was undertaken and examined experimentally.

An analysis of the input circuit of a one-port parametric amplifier (using a simplified series-equivalent circuit) was performed, from which phase shift versus frequency as a function of gain was obtained. Measurements made on the phase-shift characteristics of a C-band nondegenerate amplifier for several gain conditions were compared with the predictions of the simplified model, and they compared favorably. In addition, a relatively rigorous expression was derived for the amplifier input impedance based upon an accurate series equivalent circuit. This expression has been programmed for a Recomp II digital computer.

TABLE OF CONTENTS

LIST OF ILLUSTRATIONS

I. INTRODUCTION

Airborne Instruments Laboratory (AIL) is required to study, design, and develop:

1. Low-level solid-state limiters covering the 400 to 800 Mc range,
2. Three-port circulators covering the 4 to 8 Gc range,
3. Low-noise solid-state C-band amplifiers suitable for use in pulse-compression radar systems.

Of the total funds allotted for this program, about 65 percent have been expended. The progress of the work to date is satisfactory, and the program will be concluded with the allotted funds. A list of key personnel assigned to this contract and the total number of hours spent by each during this quarter follows:

	Hours
S. Hamilton	408
W. W. Heinz	135
S. Okwit	185
E. W. Sard	269
K. Siegel	339

II. BROAD-BAND SOLID-STATE LIMITERS FOR RECEIVER PROTECTION

The purpose of this task is to investigate solid-state limiter techniques that are capable of protecting receivers operating in the 400 to 800 Mc range. Two basic types of limiters were considered--ferrite and varactor.

A. FERRITE LIMITERS

During this report period, further investigations were made to determine whether single crystal gallium-substituted yttrium-iron garnet (Ga-YIG) with a sufficient amount of Ga substitution to yield coincidence limiting in the UHF region can be obtained without distroying the narrow linewidth properties.

Previous work on Ga-YIG, having a $4\pi M_s$ of 420 gauss, has shown that the Ga doping level required to yield the 420 gauss saturation magnetization resulted in an excessively broadened linewidth (30 oersteds) and high first- and second order anisotropy constants (reference 1). This precluded the use of Ga-YIG in low threshold-level limiters. Consequently, a less heavily doped Ga-YIG sphere having a $4\pi M_s$ of 600 gauss was purchased from Microwave Chemicals Laboratories. The sphere diameter was relatively small (0.061 inch); however, it was large enough for linewidth and anisotropy measurements. Initial measurements taken at 835 Mc have shown substantially reduced anisotropy and improved linewidth. The measured linewidths varied from 3.7 oersteds along the hard axis of the crystal to 7.8 oersteds along the easy axis. This linewidth data, unlike the previous measurements on the 420 gauss crystal reported in reference 1, behaves normally--that is, the linewidths are maximum along the easy axis and minimum along the hard axis.

To check the measured linewidth data, a series of measurements were made on the decline of susceptibility. The critical threshold power level was found to be 60 microwatts along the easy axis. This agrees well with the theoretical value of 75 microwatts.

During the next report period an attempt will be made to construct a limiter, using this 0.061-inch sphere, in a half-wavelength cross-resonator structure. It is expected that limiting levels in the region of -20 to -25 dbm will be obtained. However, the insertion loss may be of the order of several db because of the small sphere size.

B. UHF VARACTOR LIMITER

1. GENERAL

One of the attractive features of single-crystal ferrimagnetic limiters is the extremely low threshold-limiting level typically -20 to -30 dbm. Varactor limiters are not generally respected for their limiting levels; the parametric-type configurations yield thresholds of about 0 dbm. However, varactor diodes can yield relatively low power-limiting levels (-20 to -25 dbm) by using high-Q cavity configurations. The work performed during this report period concentrated on this approach--that is, obtaining a varactor-limiting configuration that yielded -20 to -25 dbm thresholds.

2. LOW-THRESHOLD VARACTOR LIMITER

By using a varactor diode mounted in a highly regenerative circuit, such as a single-tuned cavity, relatively low threshold-limiting levels can be obtained. In this configuration, the build-up of the RF field causes the diode average capacitance to increase, thereby detuning the cavity from its initial center frequency. This is a narrow-band device in which bandwidth is traded for limiting level.

The limiting characteristic of a diode-loaded quarter-wave resonator, with the diode placed in the middle of a slab-line structure, is plotted in Figure 1. The position of the diode is a compromise between low limit level and small-signal insertion loss. From this data, measured at 257 Mc, it can be seen that the device has a threshold level below -20 dbm, a dynamic range of greater than 40 db, and an insertion loss of 1.8 db. We believe that this insertion loss can be reduced because 1.3 db is contributed by the losses of the unsilvered brass resonator. The limiter can be easily tuned over an octave bandwidth and has an instantaneous bandwidth of about 2 Mc.

Figure 2 shows the limiting characteristic obtained when the diode is placed at the open end of the resonator, at the point of maximum E field. From Figure 2, it can be seen that the threshold level decreased to below -25 dbm, and the insertion loss increased to 4 db.

The equivalent circuit of the limiter, when referred to the diode location at the high-impedance point in the cavity, is shown in Figure 3. The cavity is represented as a parallel resonant circuit with ideal transformers accomplishing the input and output coupling. R_D is the equivalent shunt-diode loss resistance, and R_C is that of the cavity. The conditions determining the operating point can be seen from Figure 4. The diode capacitance, and, therefore, the total capacitance are functions of the RF voltage across them (Figure 4A). The response of the resonant circuit with total capacitance at a fixed frequency is shown in Figure 4B for various levels of input voltage E. Since both conditions must be satisfied, the points of intersection are the operating points. The solid curve in Figure 4B is adjusted for small-signal resonance. Detuning can be seen with input power. However, other tuning conditions, such as the dashed curve on the left in Fig-

ure 4B, can have multiple intersections, which result in discontinuous jumps in the operating points when the circuit is tuned by varying the frequency (in this case) or the bias (in general). It can be seen that this sort of behavior occurs when the curvature of the C_{TOT} versus V_d curve is relatively large and the resonant circuit has a high Q. It should be noted that these jumps have been observed in varactor frequency multipliers and can occur in the pump circuits of parametric amplifiers.

Referring to Figure 3, using the end-loaded cavity with signals small enough not to cause diode conduction, and neglecting cavity loss, the insertion loss is:

$$L = \left(1 + \frac{1}{2} Z_0^1 Y\right)^2$$

where

$Z_0^1 = n^2 Z_0$

n = transformation ratio

and

$$Y = G + j\left(\omega C_{TOT} - \frac{1}{\omega L}\right)$$

where

diode loss conductance $(G) = \frac{1}{Q_d^2 R_s} = \omega^2 C_j^2 R_s$

where

R_s = diode series resistance,

C_j = junction capacitance.

When initially adjusted for resonance

$$Y = \omega^2 C_j^2 R_s + j\omega\,(\Delta C_j)$$

where ΔC_j = the change in the junction capacitance with pumping, and

$$|Y| = \left[\left(\omega^2 C_j{}^2 R_s\right)^2 + \omega^2\left(\Delta C_j\right)^2\right]^{1/2}$$

The insertion loss is then

$$L = 1 + \tfrac{1}{4} Z_0^{1^2}\left[\left(\omega^2 C_j{}^2 R_s\right)^2 + \omega^2\left(\Delta C_j\right)^2\right] + Z_0^1\left[\left(\omega^2 C_j{}^2 R_s\right)^2 + \omega^2\left(\Delta C_j\right)^2\right]^{1/2}$$

But C_j is a function of (V_d), and

$$V_d = \left(P_{out}\ Z_0^1\right)^{1/2}$$

Thus,

$$C_j = f'\ (P_{out})$$

and

$$P_{out} = \frac{P_{in}}{L}$$

Once the parameters are known, values for V_d can be assumed and P_{out} versus P_{in} can be calulated (subject to the restrictions of the simple model).

The calculated input-output curve is shown in Figure 5 for two assumed values of the transformation ratio, n = 20 and n = 56. For n = 20, the theoretical 3 db departure from linearity is -26 dbm, agreeing favorably with the measured data in Figure 2. However, the measured insertion loss is about 2 db greater than expected, because some of the parameters may be slightly in error. Calculations were per-

formed only for voltages of up to 0.5 volt at the diode, where conduction of the junction and enormous waveform asymmetry make the linearized calculation oversimplified. Near this point, the large junction admittance clamps the diode voltage on the forward half cycle and peaks the voltage on the reverse portion. For this reason, two diodes, with opposite polarities, should yield greater attenuation at higher power levels, but the small-signal loss would also be increased.

The simple model for the end-loaded cavity previously discussed does not predict any decrease in the output as the input increases--that is, the cavity-transformation ratio remains constant as the field configuration shifts. Moreover, a decreasing output that is caused by an increase in diode admittance, with any mechanism except negative resistance, requires an increase in diode voltage, and, therefore, a corresponding increase and not a decrease in output power (Figure 2). For the case shown in Figure 1 however, with the diode location at a point other than the high-impedance point, the diode voltage is not a direct transformation of the voltage across the output and, therefore, may increase as the output decreases. Because of the complexity of the large-signal phenomena for this device, the previous explanations are merely suggestions of possible behavior.

3. ULTRA-LARGE DYNAMIC RANGE LOW-THRESHOLD LIMITER

The capabilities of a cascaded varactor limiter system consisting of the higher-threshold level broad-band device described in reference 1 followed by the previously described low-threshold level limiter can be considered. The limiting characteristic of this system is shown in Figure 6. The dynamic range is in excess of 70 db, the threshold level is less than -20 dbm, and the overall insertion loss is 2 db. In addition, this system should be capable of handling incident energy up to 87,000 ergs. To our knowledge, this system has the largest dynamic range and lowest threshold characteristic of any varactor limiter system.

III. 4 TO 8 GC CIRCULATOR

The purposes of this task are to develop a design theory for a strip-transmission-line Y-junction broad-band circulator, and to design and construct two breadboard models of a fixed-tuned circulator covering the 4 to 8 Gc range.

The investigation of the performance of the Bendix C-band strip-transmission-line circulator as predicted by Bosma's analysis (reference 3) was initiated. The necessary modifications in the equations were made for negative values of μ_{eff} and an extended frequency variation. At the same time, the effect of imperfectly matching a circulator by the technique described in reference 1 was analyzed. The Bendix C-band circulator was modified further to use a double-tuned matching network, and partial success was achieved.

A. THEORETICAL PERFORMANCE OF BENDIX C-BAND CIRCULATOR (PRELIMINARY)

The Bendix C-band circulator mentioned in Section III of reference 1 is not constructed exactly like the model analyzed by Bosma. In particular, the three center conductors taper to a smaller width just outside the ferrite disks and then are simply joined in the middle of the disks. Bosma assumes that the three center conductors are joined to the outer edge of a metal disk completely overlapping the ferrite disks. Nevertheless, it is of interest to apply Bosma's theory (reference 4) to the Bendix circulator using the frequency variation of ferrite parameters derived in Appendix A.

The pertinent measured parameters for the Bendix circulator are:

R (ferrite disk radius) = 0.250 inch
t (ferrite disk thickness) = 0.093 inch

W (center conductor width) = 0.216 inch

H_a (applied magnetic field in z-direction) $\approx$ 1200 oersteds

f_o (center frequency) = 5500 Mc

For calculating the magnetization and effective internal field, the demagnetization factors $N_x = N_y$, and N_z are required. Assuming that these values are approximately the same as those for an ellipsoid of the same dimensions, these values are (Figures 1 and 3 of reference 5):

$$\frac{N_x}{4\pi} = \frac{N_y}{4\pi} \approx 0.115$$

$$\frac{N_z}{4\pi} \approx 0.77$$

The magnetization in the z-direction is (equation 4.4 of reference 5):

$$4\pi M = \frac{H_a}{\frac{N_z}{4\pi} + \frac{1}{\chi_z}} \approx \frac{H_a}{\left(\frac{N_z}{4\pi}\right)} \quad \chi_z >> 1 \qquad (1)$$

where χ_z is the z-component of magnetic susceptibility. In addition, the effective internal field in the z-direction is (reference 6):

$$H_i = H_a + \left(\frac{N_x}{4\pi} - \frac{N_z}{4\pi}\right) 4\pi M \qquad (2a)$$

(substituting equation 1)

$$\approx H_a \left[\frac{\left(\frac{N_x}{4\pi}\right)}{\left(\frac{N_z}{4\pi}\right)}\right] \qquad (2b)$$

Thus, from equations A-3 (Appendix A), 1, and 2b, and the ferrite parameters previously described, the normalized center frequency values of magnetization and effective internal field are:

$$m_0 = \frac{\gamma(4\pi M)}{\omega_0} = 0.794$$

$$h_0 = \frac{\gamma H_i}{\omega_0} = 0.09$$

Furthermore, from equation A-4 (Appendix A), the center frequency value of effective permeability is:

$$(\mu_{eff})_0 = 1 - \frac{m_0(m_0 + h_0)}{1 - h_0(m_0 + h_0)} = 0.238$$

From equation 13 of reference 4, the center value of parameter x is ($\epsilon = 15$)

$$x_0 = \frac{2\pi R}{\lambda_0}\sqrt{\epsilon(\mu_{eff})_0} = 1.38$$

From equation 12 of reference 4 and equation A-5 of Appendix A, the center value of parameter y is

$$y_0 = -\frac{1}{x_0}\left[\frac{m_0}{1 - h_0(m_0 + h_0)}\right] = -0.625$$

The last parameter required is the half angle ψ (Figure 10-B of reference 4) subtended by the center conductor at the edge of the ferrite disk. This value is:

$$\psi \approx \left(\frac{W}{R}\right)\left(\frac{90}{\pi}\right) = 25 \text{ degrees}$$

From the inequality following equation A-9 (Appendix A), $\mu_{eff} < 0$ for $0.282 < f' < 0.884$. It is this broad frequency range that is being investigated on the computer using the previously established values of x_0, y_0, $(\mu_{eff})_0$, and ψ, the frequency variation relations in Appendix A and the adaptation to $\mu_{eff} < 0$ in Appendix B.

B. EXPERIMENTAL MODIFICATIONS OF BENDIX CIRCULATOR

It is pertinent to give some additional measured performance data on the original Bendix circulator and on the circulator with the modified dielectric rings (reference 1). Figure 7 shows data that is similar to that shown in Figure 14 of reference 1 for the same circulator ports. The essential difference in conditions for both figures is that a better matched load was used in the latest measurements, which especially improved the mid-band isolation of the modified circulator. Furthermore, continuous instead of discrete frequency measurements reveal resonances in the responses of both circulators at about 5.0 and 6.2 Gc. The resonance at 6.2 Gc had been noted only on the modified circulator forward loss curve of Figure 14 of reference 1. Even in the latest measurements, however, the improvement in performance is not as great as expected, particularly at the low end of the frequency range. This can be seen from the equations derived in Appendix C for the effect of imperfect matching on circulator performance. Referring to Figures 12 and 13 of reference 1, the distance between desired and actual matching loci $|\delta|$ for

the modified circulator is less than that for the original circulator at both ends of the range. Thus, from equation C-7b (Appendix C), the isolation should be improved at both ends of the frequency range, instead of at the high end only.

Various other partially successful modifications of the Bendix circulator have been tried during the last report period. A typical example--matching with a two-section quarter-wavelength transformer--is described on the following pages. Figure 8 shows the desired matching locus, measured in the same way as in reference 1, for the Bendix circulator with a modified center conductor. To explain the modification, each center conductor near the terminals of the original Bendix circulator has a width that corresponds approximately to a 50-ohm impedance. The center conductor then starts to taper in width so that it corresponds to a higher impedance a short distance away from the edges of the ferrite disks.* The taper ends at the edges of the disks, and the center conductor has a constant width within the disk region. The modification to the center conductor eliminated the tapered section by lengthening the 50-ohm line up to the edges of the ferrite disks and then abruptly reducing the width to the original value inside the disk region. It was then possible to obtain the rotated desired locus, shown in Figure 8, at a reference plane about 0.056 inch from the edges of the disks.

---

* The inner edges of the original dielectric rings were located at the point where the taper started. Thus, referring to Figure 12 of reference 1, it was impossible to rotate the desired matching locus for the original Bendix circulator until it was conveniently centered on the negative real axis of the Smith chart.

Also shown in Figure 8 is the theoretical locus corresponding to a two-section quarter-wavelength transformer designed according to Appendix D with the parameters $s_0 = 5/3$, $s_1 = 2$, and $f_0 = 5.3$ Gc. Table I shows the values of isolation calculated from equation C-7b. The values of $|\delta|$ (equivalent

TABLE I

CALCULATION OF ISOLATION FOR MATCHED BENDIX C-BAND CIRCULATOR WITH MODIFIED CENTER CONDUCTOR

Frequency (Gc)	$\|\delta\|$ (Equivalent SWR)	$\|\delta\|$	$\|S_{12}\|^2$ (db)	$\|S_{13}\|^2$ (db)	$\left\|\frac{S_{12}}{S_{13}}\right\|^2$	Isolation (db)
3.2	1.65	0.245	--	--	--	--
3.6	1.3	0.13	--	--	--	--
4.0	1.12	0.0567	-9	-1	0.16	23
4.4	1.09	0.043	-10	-1.5	0.14	26
4.8	1.13	0.061	-11.5	-1	0.09	23
5.2	1.16	0.074	-11.5	-0.5	0.08	22
5.6	1.1	0.0476	-20	-0.5	0.01	26
6.0	1.17	0.0784	-10	-0.5	0.11	21
6.4	1.18	0.0826	-12	-4	0.16	20
6.8	1.17	0.0784	-10	-4	0.25	20
7.2	1.5	0.2	-8	-3	0.32	11
7.6	1.84	0.296	-8	-4	0.40	6

SWR) were read directly from Figure 8 by marking the distances between corresponding points on the two loci on the real axis. Furthermore, the values of $|S_{12}|^2$ and $|S_{13}|^2$ were estimated from the swept frequency responses in Figure 9 for the circulator that was not matched. More simply, $|S_{12}/S_{13}|^2$ could have been read directly from the desired matching locus in

Figure 8 since, theoretically, $|S_{12}/S_{13}| = |\rho|$ (equation I-10 of reference 1). It can be seen that approximately 20 db or greater isolation is predicted between 3.8 to 6.8 Gc. The actual transformer was constructed using one pair of dielectric rings with $\epsilon = 4$ a half-wavelength wide. Enough of the original width of the center conductor was cut away to make the impedances of each section theoretically equal to 80.3 and 62.3 ohms in air. With the dielectric, this corresponded to values of $Z_1 = 40.2$ and $Z_2 = 31.2$ ohms calculated from equation D-4 and the previously mentioned values of s_0 and s_1. Figure 10 shows the resulting circulator performance. The expected isolation was achieved only at the low end of the band.

C. FUTURE PLANS

It is hoped to complete the calculation of performance of the Bendix circulator as predicted by Bosma's analysis.

The reasons for only partial success in matching the circulators over a wide band will be investigated. In particular, a strip-transmission-line slotted section will be constructed to measure a duplicate of the transition between the strip-transmission line and the coaxial connector in the Bendix circulator. Measurements will also be made on duplicates of the matching networks, to determine if their theoretical reflection coefficient loci are actually being obtained.

IV. BROAD-BAND LOW-NOISE C-BAND AMPLIFIER

The purposes of this task are:

1. Develop a design theory for low-noise solid-state amplifiers suitable for use in C-band pulse-compression radars,
2. Design and construct a breadboard model for such an amplifier.

During the report period, an analysis of the input impedance of a one-port parametric amplifier, using a simplified series equivalent circuit (nonfrequency dependent, negative resistance) was performed. From this analysis information on phase shift versus frequency as a function of amplifier gain was obtained. A detailed set of phase measurements were then made on a balanced C-band nondegenerate amplifier, for several gain conditions, and compared with predictions of the simplified model. In addition, a relatively rigorous expression was derived for the amplifier input impedance, based upon what is believed to be an accurate series equivalent circuit. This expression is in the process of being programmed for a Recomp II digital computer.

A. SIMPLIFIED THEORY

To obtain a qualitative picture of the phase shift of a one-port parametric amplifier, a simplified equivalent circuit (Figure 11) has been analyzed. This circuit assumes that the negative resistance (-R) is frequency independent, which is unquestionably contrary to fact. However, the results obtained from this model are believed to be of qualitative value, as well as some quantitative value. In addition, the analysis is worthwhile presenting, in view of the application of the duality of the proposed model to tunnel diodes.

From Figure 11, the reflection coefficient (Γ) of a one-port parametric amplifier being driven from an ideal lossless circulator is:

$$\Gamma = \frac{-R + j(\omega L - \frac{1}{\omega C}) - R_0}{-R + j(\omega L - \frac{1}{\omega C}) + R_0} \tag{3}$$

where

$-R$ = diode negative resistance (frequency independent),
R_0 = transformed generator impedance seen by the diode,
L = total circuit inductance,
C = total stray and junction capacitance.

Equation 3 can be put into the form:

$$\Gamma = -\left[\frac{\frac{2\sqrt{G_0}}{1 + \sqrt{G_0}} - jx}{\frac{2}{1 + \sqrt{G_0}} + jx}\right] \tag{4}$$

where

$\sqrt{G_0}$ = voltage gain of the center frequency = $\left|\frac{1 + \frac{R}{R_0}}{1 - \frac{R}{R_0}}\right|$

$$x = \frac{1}{2\pi f_0 R_0 C}\left(\frac{f}{f_0} - \frac{f_0}{f}\right)$$

f_0 = center frequency = $\frac{1}{2\pi\sqrt{LC}}$

f = operating frequency.

The resulting phase shift is found to be:

$$\measuredangle\Gamma = \pi - \tan^{-1}\left[\frac{2x}{\frac{4\sqrt{G_0}}{(1+\sqrt{G_0})^2} - x^2}\right] \tag{5}$$

From equation 4 the value of x at the 3-db points ($x_{3\ db}$) is found to be:

$$x_{3\ db} = \pm\frac{2\sqrt{G_0}}{(1+\sqrt{G_0})(\sqrt{G_0}-2)} \tag{6}$$

Substituting equation 6 into 5 yields the phase shift at the 3-db points:

$$(\measuredangle\Gamma)_{3\ db} = \pi \mp \tan^{-1}\left[\frac{\sqrt{G_0}-2}{\sqrt{G_0}-2}\right] \tag{7}$$

This expression is an interesting result, and is plotted in Figure 12. It shows that, for the low gain condition, the amplifier phase shift is greater than the expected conventional 45 degrees, and asymptotically approaches 45 degrees with increasing gain. A possible explanation of this is believed to be in the relative influence that an incident and reflected wave of different amplitude has on the reflection coefficient.

From equation 5 a general plot of the amplifier phase-shift characteristic can be obtained as a function of

frequency and gain. However, to plot the equation in a meaningful form, a frequency normalizing factor $(\frac{f}{B})$ is introduced, where B is the 3-db bandwidth. From the previously defined terms we obtain:

$$\frac{\Delta f}{B} = \frac{f - f_0}{B} = \frac{\frac{1}{2}\left(xR_0\sqrt{\frac{C}{L}} + \sqrt{x^2R_0^2\frac{C}{L} + 4}\right) - 1}{x_{3\ db}\,R_0\sqrt{\frac{C}{L}}} \qquad (8)$$

Using the first two terms of the power series expansion of $(x^2R_0^2\frac{C}{4} + 4)^{1/2}$ we get the approximation:

$$\frac{\Delta f}{B} \approx \frac{x}{Rx_{3\ db}}\left[1 + \frac{x}{4}R_0\sqrt{\frac{C}{L}}\right] \qquad (9)$$

With equations 5, 6, and 9, the general normalized phase-shift characteristic can be plotted (Figure 13). The constants chosen for this plot are representative of the actual balanced amplifier used to obtain experimental data (presented in the next section). These values are, C = 1.8 μμf, f_0 = 5.5 Gc, and R_0 = 14.4 ohms. A discussion of Figure 13 is included in the following section, in which comparisons are made to the measured data.

B. PHASE SHIFT MEASUREMENTS

An amplifier similar to the one described in reference 1 was designed to operate at 5.5 kMc. The amplifier was a single-tuned, balanced, nondegenerate, one-port parametric amplifier being fed by a Bendix circulator (described in Section III). The amplifier configuration is of a form factor that will enable multiple tuning to be easily incorporated when required. The amplifier-circulator package and an open view of the balanced diode mounting are shown in Figure 14.

A series of measurements were made on the phase characteristics of this amplifier under two different gain conditions, 20 db and 13 db (using a slotted-line phase bridge technique). A plot of the measured data is shown in Figure 15. Comparison of the experimental and theoretical data in Figures 12, 13, and 15, show surprisingly good agreement. This is clearly seen in the tabulated data of Tables II and III. Table II compares the measured and expected phase shift at the half-power points, and Table III compares the expected deviation of the phase shift from linearity to the measured deviation.

TABLE II

EXPECTED AND MEASURED PHASE SHIFT AT THE 3-DB POINTS

G_0 (db)	$(\measuredangle\Gamma)_{3\ db}$ Measured (degrees)	$(\measuredangle\Gamma)_{3\ db}$ Calculated (degrees)
13	55	59
20	50	51

TABLE III

PHASE-SHIFT DEVIATION FROM LINEARITY

$\left(\frac{2\Delta f}{B}\right)$ for a given percent deviation from linearity

G_0 (db)	±2-1/2 Percent Measured	±2-1/2 Percent Calculated	±5 Percent Measured	±5 Percent Calculated
13	0.66	0.57	0.84	0.70
20	0.74	0.61	0.97	0.75

It should be emphasized that the good agreement of the theoretical and experimental data are on a normalized basis only. The operating bandwidth predicted by the simplified model is an order of magnitude greater than the measured data yielded by the amplifier. This poor correlation is a result of the erroneous assumption of a frequency independent negative resistance, and neglect of the parametric lead inductance. The predicted bandwidth, however, is consistent with tunnel-diode amplifiers, which in fact do have a constant negative resistance.

In view of this poor correlation, a program was initiated to obtain a more exact expression of the amplifiers input impedance, using what is believed to be a relatively accurate equivalent circuit (Figure E-2 of Appendix E). The derived expression (Appendix E, equation E-4) is presently being programmed on a Recomp II digital computer. It is believed that the results of this analysis, which will be included in the next quarter report, will yield a greater degree of correlation to the measured data--specifically the bandwidth characteristics.

V. REFERENCES

1. S. Hamilton et al., "Second Quarterly Progress Report on Solid-State Circuits," Report No. 1654-I-2, AIL, Deer Park, N. Y., October 1962.
2. J. C. Greene et al., "Application of Semi-Conductor Diodes to Microwave Low-Noise Amplifiers and Harmonic Generators," Report No. 5872-1, AIL, Deer Park, N. Y.
3. H. Bosma, "On the Principle of Stripline Circulation," Proceedings of the Institute of Electrical Engineers, Part C, p 137-146, January 1962.
4. J. C. Greene et al., "First Quarterly Progress Report on Solid-State Circuits," Report No. 1654-I-1, AIL, Deer Park, N. Y., July 1962.
5. J. A. Osborn, "Demagnetizing Factors of the General Ellipsoid," Physical Review, Vol 67, No. 11 and 12, p 351-357, 1 and 15 June 1945.
6. C. L. Hogan, "The Ferromagnetic Faraday Effect at Microwave Frequencies and its Applications - The Microwave Gyrator," Bell System Technical Journal, Vol 31, p 1-31, January 1952.
7. S. Ramo and J. R. Whinnery, "Fields and Waves in Modern Radio," Second Edition, John Wiley and Sons, Inc., New York, 1953.
8. T. Hyltin, "Varactor Packaging and Paramp Performance," Microwaves, Hayden Publishing Co., July 1962.
9. G. Matthaei, "A Study of the Optimum Design of Wide Band Parametric Amplifiers and Up-Converters," PGMTT, p 23, January 1961.

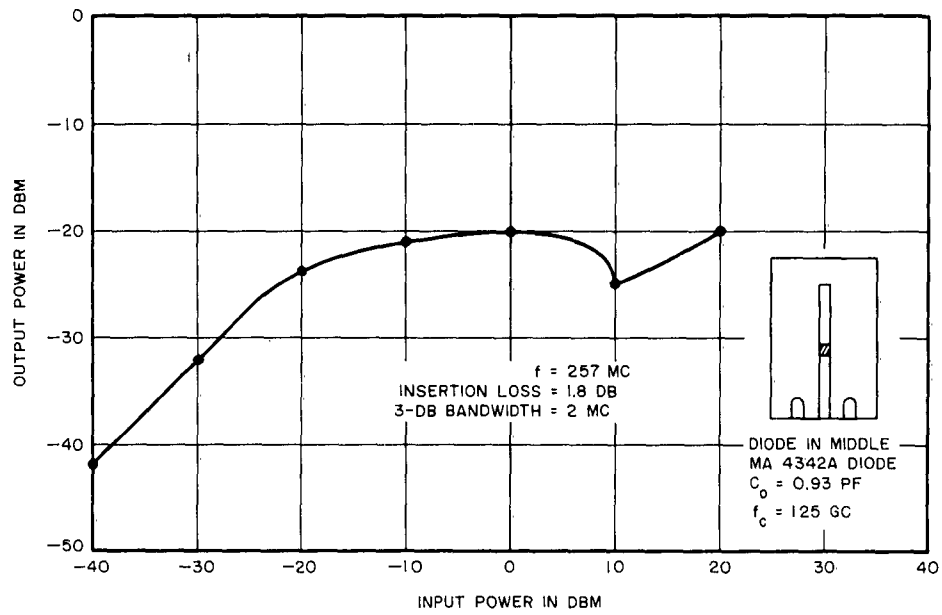

FIGURE 1. LIMITING CHARACTERISTIC OF DIODE-LOADED QUARTER-WAVE RESONATOR WITH DIODE PLACED IN MIDDLE OF SLAB-LINE STRUCTURE

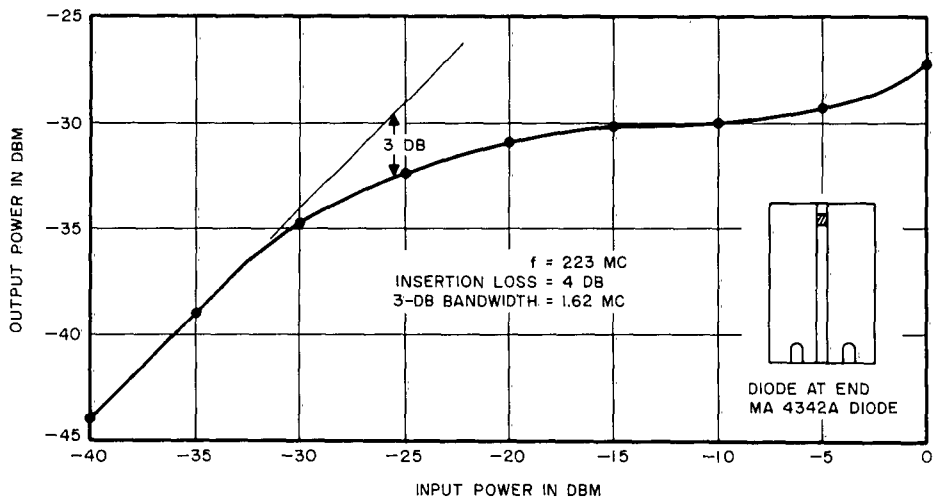

FIGURE 2. LIMITING CHARACTERISTIC OF DIODE-LOADED QUARTER-WAVE RESONATOR WITH DIODE PLACED AT END OF SLAB-LINE STRUCTURE

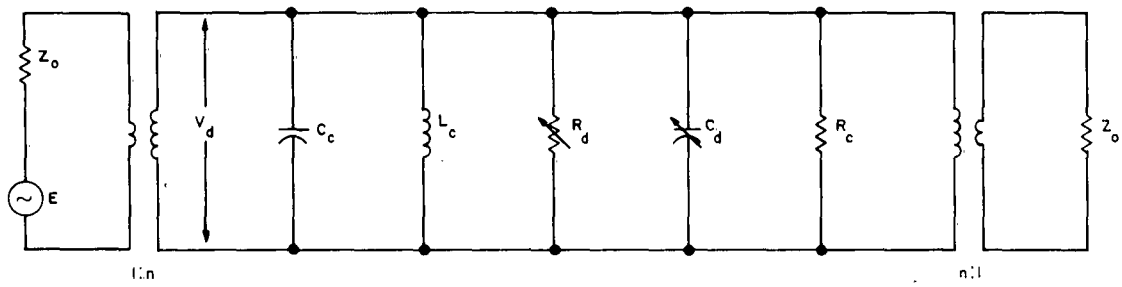

FIGURE 3. EQUIVALENT CIRCUIT OF DIODE-LOADED CAVITY (SMALL SIGNAL)

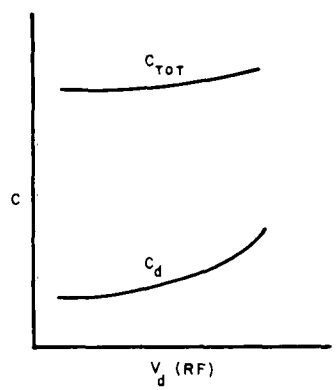

A. CAPACITANCE AS FUNCTION OF DIODE VOLTAGE

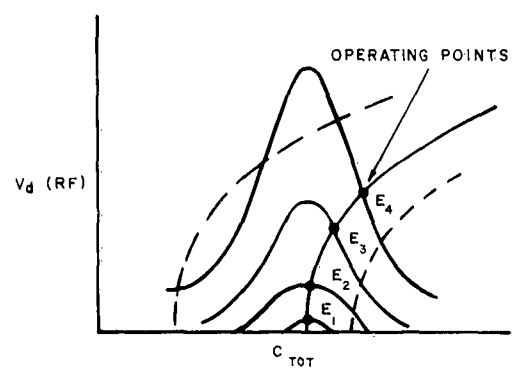

B. RESPONSE OF RESONANT CIRCUIT AND RESULTANT OPERATING POINTS

FIGURE 4. CONDITIONS DETERMINING OPERATING POINT

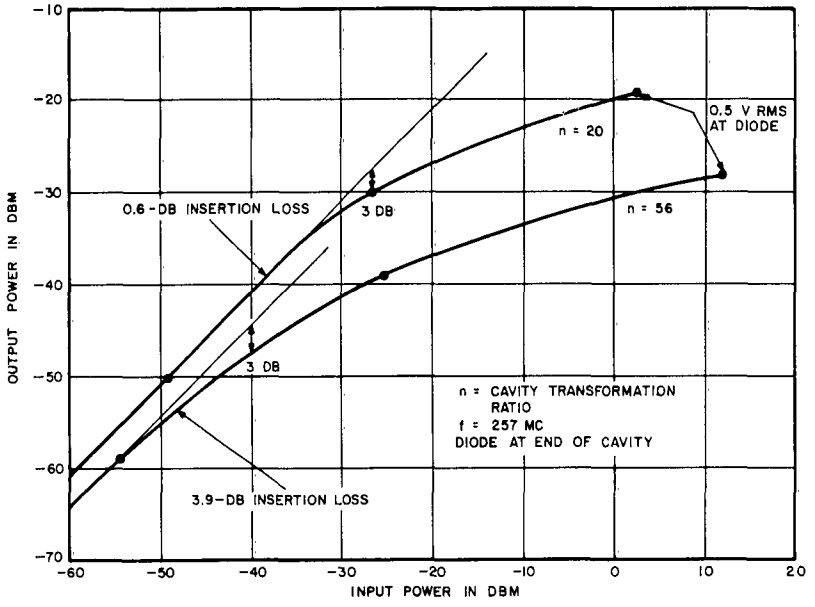

FIGURE 5. CALCULATED LIMITING CHARACTERISTIC ASSUMING LOSSLESS CAVITY

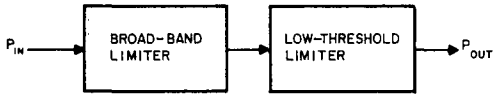

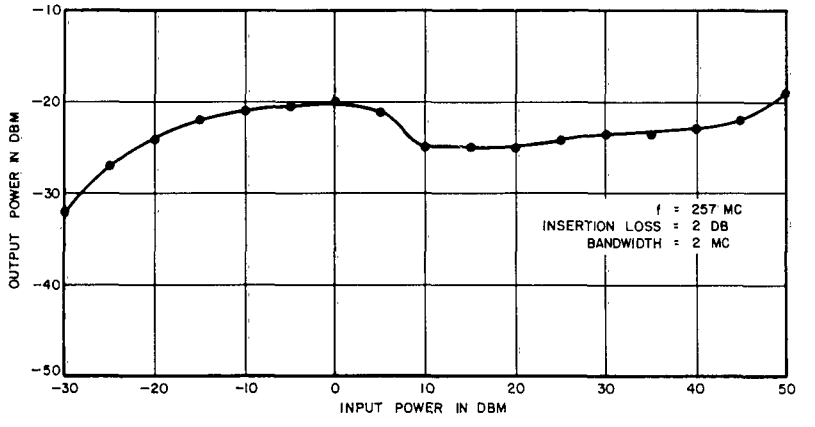

FIGURE 6. COMPOSITE VARACTOR LIMITER

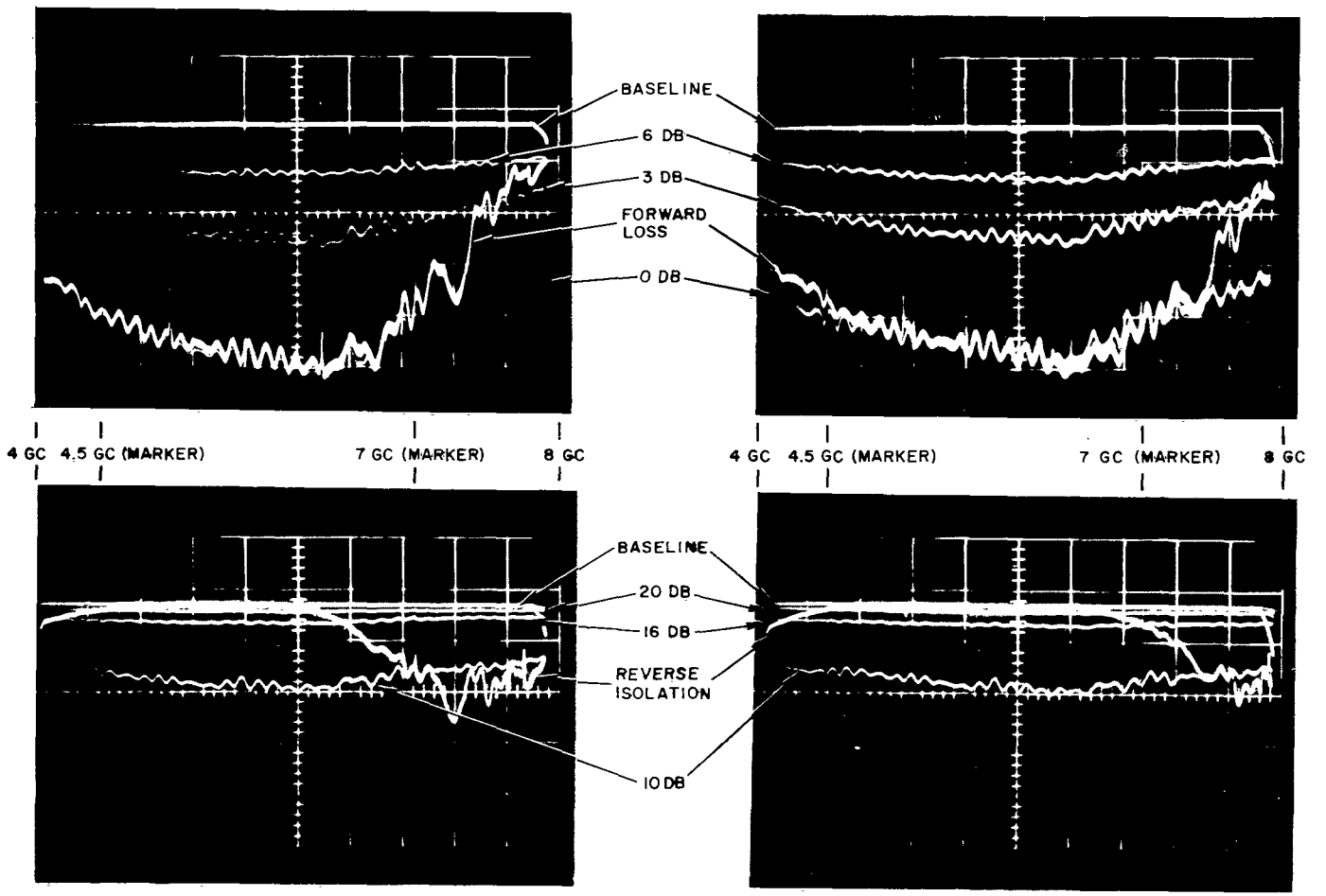

FIGURE 7. PERFORMANCE OF BENDIX C-BAND CIRCULATOR VS FREQUENCY

POINT	FREQUENCY IN GC
1	3.2
2	3.6
3	4.0
4	4.4
5	4.8
6	5.2
7	5.6
8	6.0
9	6.4
10	6.8
11	7.2
12	7.6

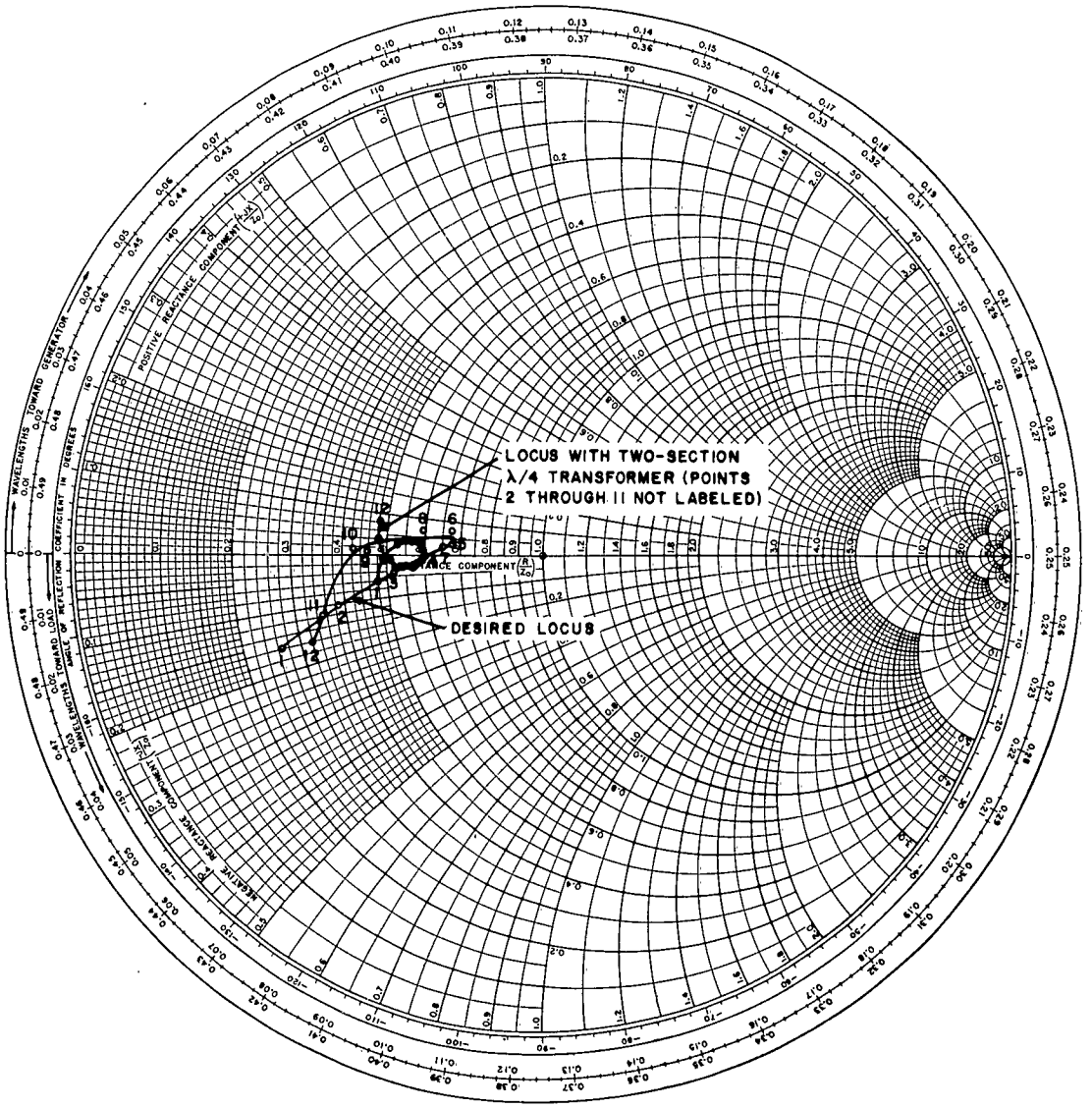

FIGURE 8. REFLECTION COEFFICIENT LOCI OF MATCHING NETWORKS FOR BENDIX C-BAND CIRCULATOR WITH MODIFIED CENTER CONDUCTOR

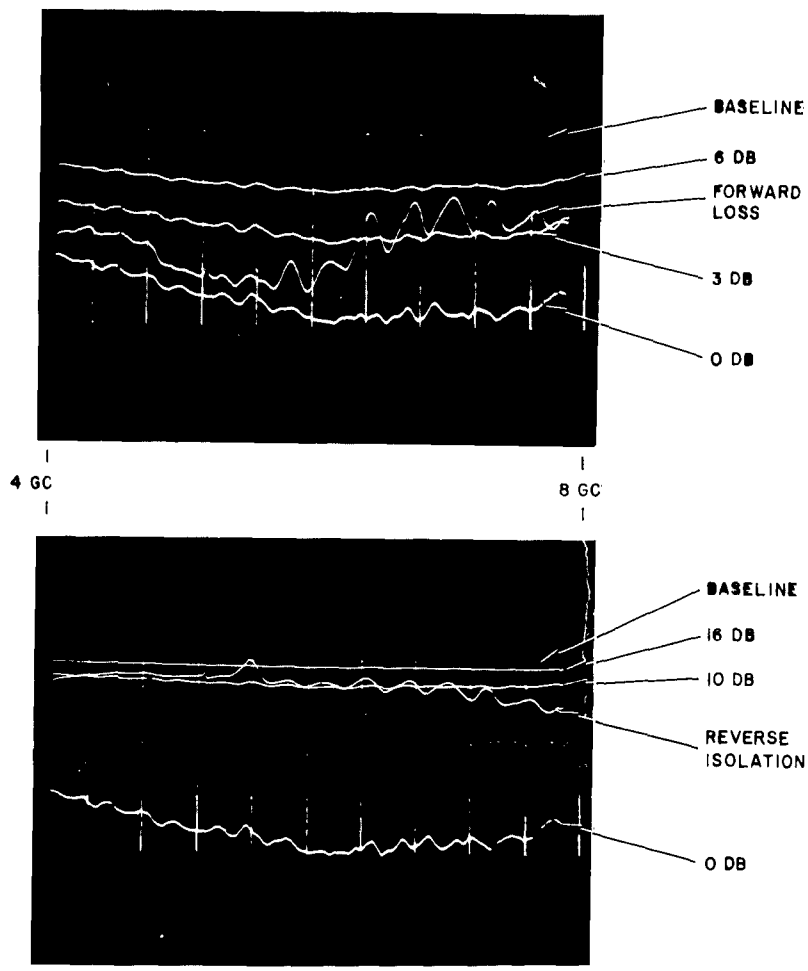

FIGURE 9. PERFORMANCE OF UNMATCHED BENDIX C-BAND CIRCULATOR WITH MODIFIED CENTER CONDUCTOR VS FREQUENCY

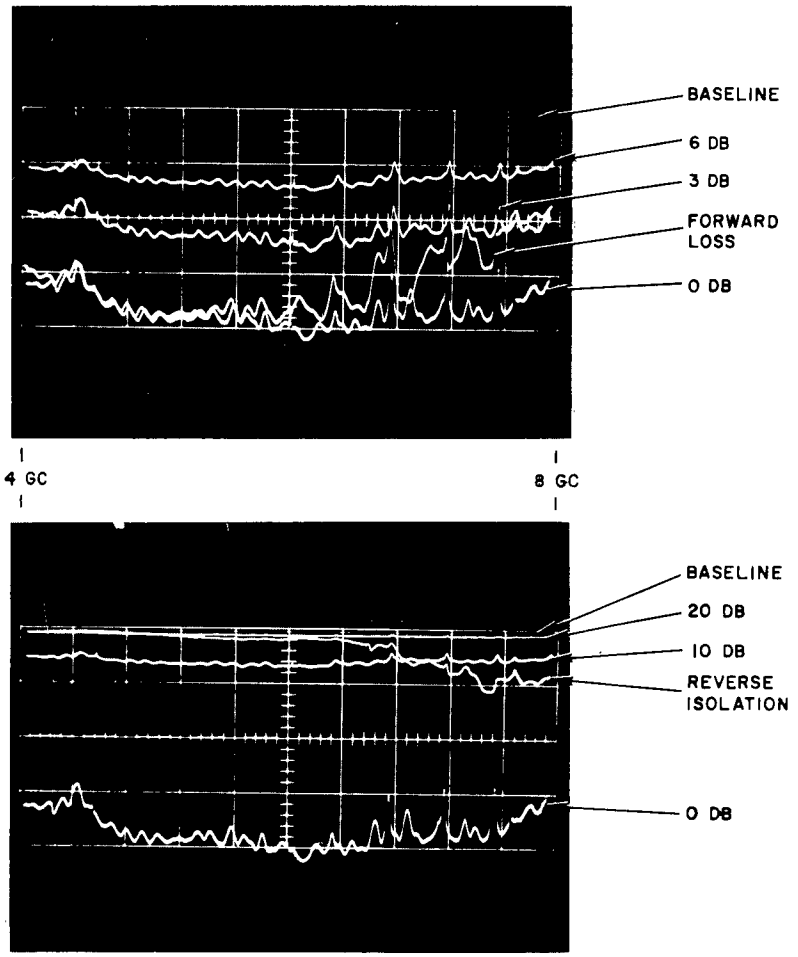

FIGURE 10. PERFORMANCE OF MATCHED BENDIX C-BAND CIRCULATOR WITH MODIFIED CENTER CONDUCTOR VS FREQUENCY

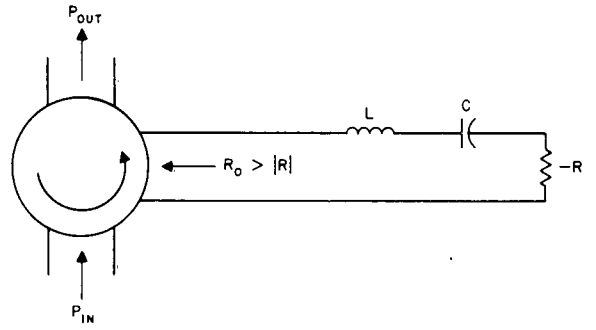

FIGURE 11. SIMPLIFIED SERIES EQUIVALENT CIRCUIT FOR ONE-PORT PARAMETRIC AMPLIFIER

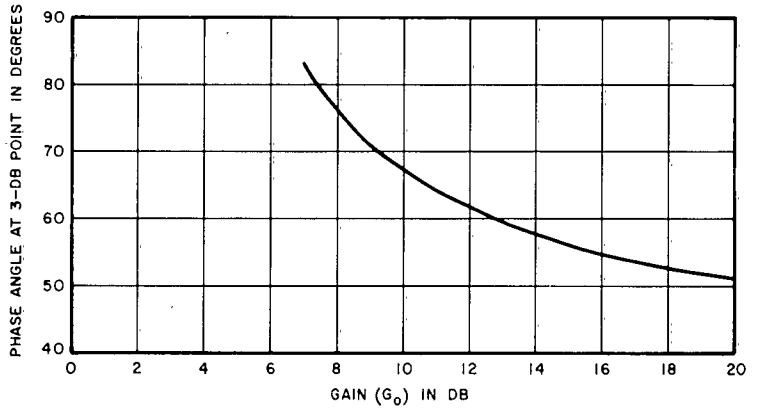

FIGURE 12. AMPLIFIER PHASE SHIFT AT 3-DB GAIN POINT AS A FUNCTION OF CENTER FREQUENCY GAIN

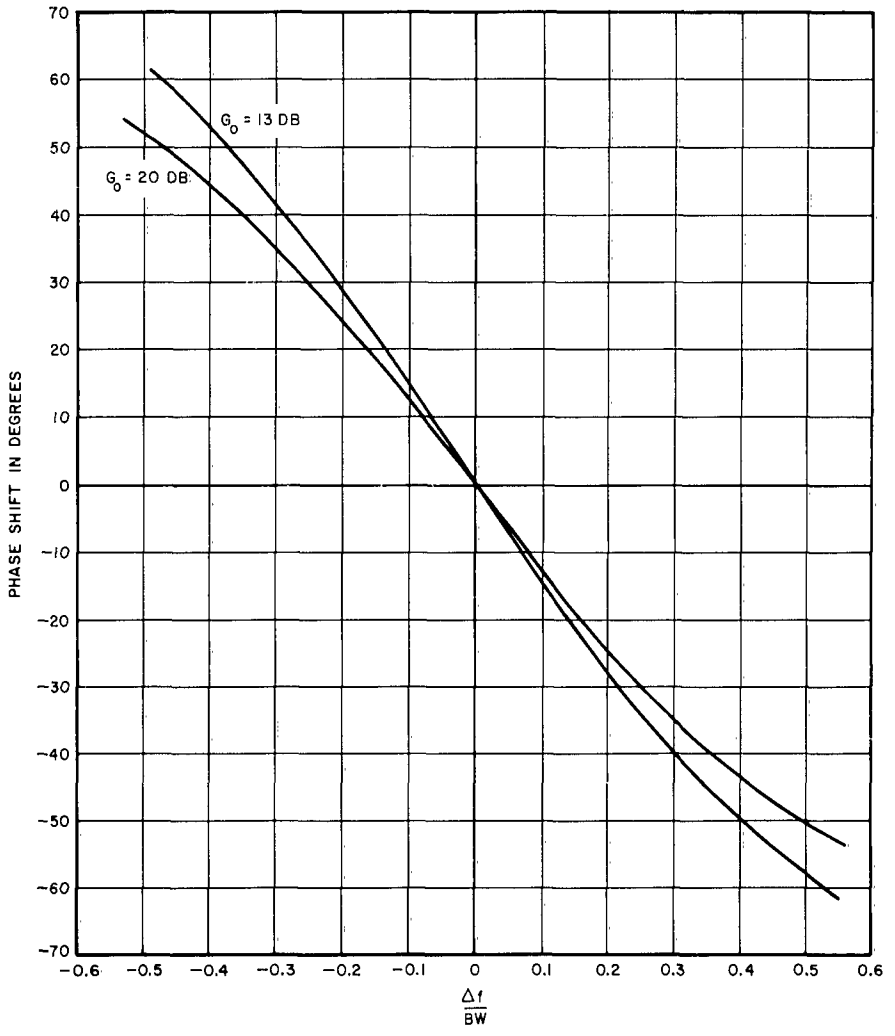

FIGURE 13. PHASE SHIFT CHARACTERISTIC VS NORMALIZED FREQUENCY AS A FUNCTION OF CENTER FREQUENCY GAIN

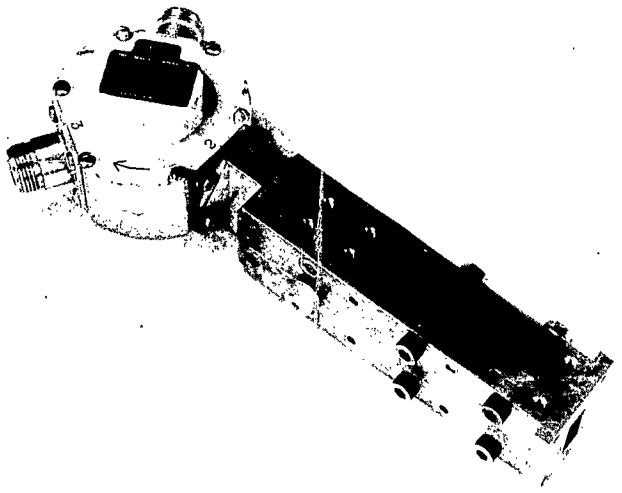

A. AMPLIFIER CIRCULATOR PACKAGE

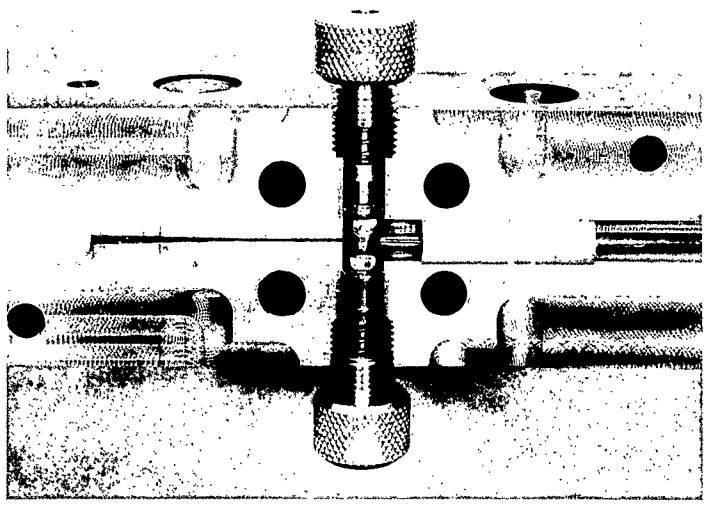

B. OPEN VIEW OF DIODE MOUNT

FIGURE 14. C-BAND NONDEGENERATE BALANCED PARAMETRIC AMPLIFIER

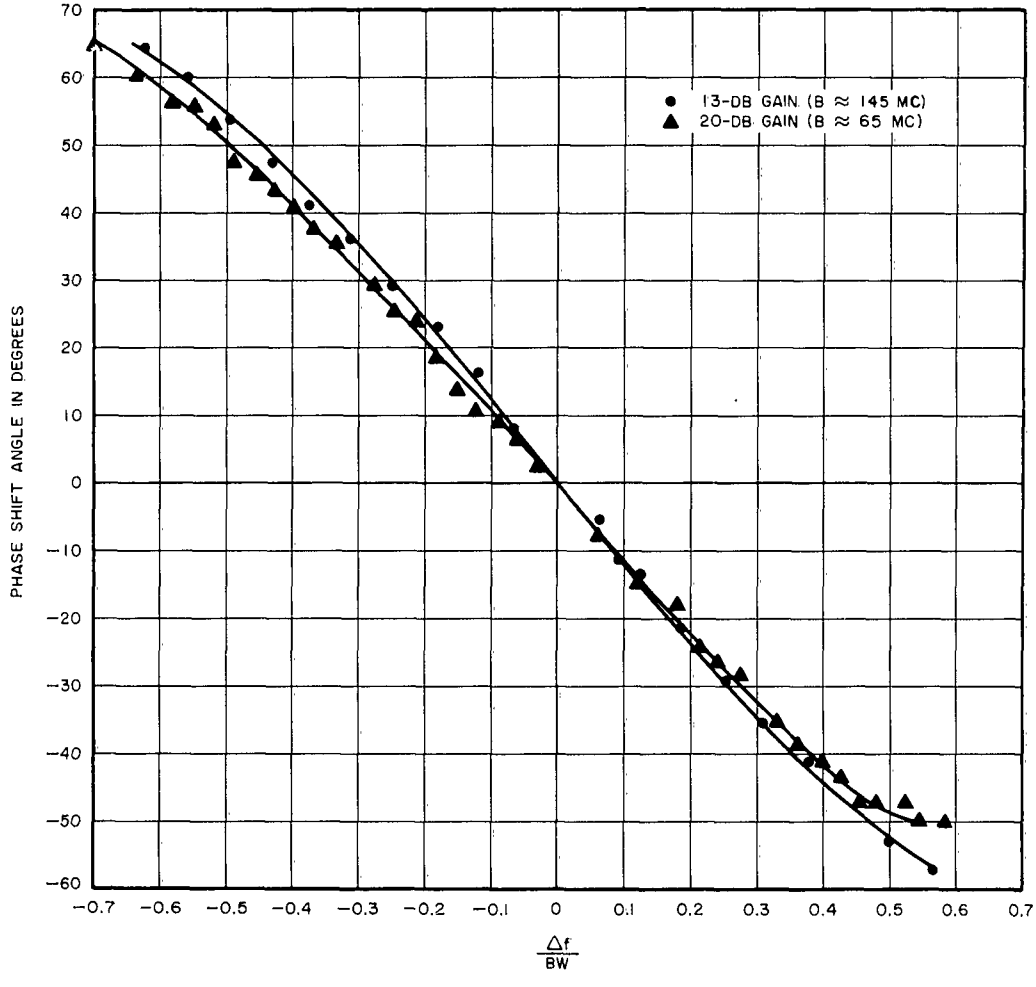

FIGURE 15. EXPERIMENTAL PHASE SHIFT VS NORMALIZED FREQUENCY AS A FUNCTION OF GAIN

APPENDIX A

EXTENDED FREQUENCY VARIATION OF FERRITE PARAMETERS FOR LOW FIELD CASE

To calculate the scattering matrix elements of the Bendix circulator as functions of frequency using Bosma's analysis (Section III, paragraph B of reference 4) values of x, y, and μ_{eff} must be calculated from the ferrite characteristics as functions of frequency. Because of the wide frequency range involved, more complete equations than equations 5 through 8 of reference 1 will be used. Going back to equations 63 and 64 of reference 3, but neglecting the ferrite line width since the operating frequency is still assumed to be high compared to the resonant frequency,

$$\mu = 1 + \frac{mh}{h^2 - 1} \tag{A-1}$$

$$k = \frac{m}{h^2 - 1} \tag{A-2}$$

where

$$m = \frac{\gamma(4\pi M)}{\omega} \tag{A-3a}$$

$$h = \frac{\gamma H_i}{\omega} \tag{A-3b}$$

and $\gamma = 2.8$ Mc/oersted is the gyromagnetic ratio, $4\pi M$ is the magnetization of the ferrite in oersteds, H_i is the effective internal magnetic field of the ferrite in oersteds, and ω is the angular frequency. Thus, the effective ferrite permeability is:

$$\mu_{eff} = \frac{\mu^2 - k^2}{\mu} = 1 - \frac{m(m + h)}{1 - h(m + h)} \qquad \text{(A-4)}$$

Also, the ratio k/μ is

$$\frac{k}{\mu} = - \frac{m}{1 - h(m + h)} \qquad \text{(A-5)}$$

Considering the variation with frequency, denote the values of quantities at $f = f_0$ by subscript 0. Thus, from equations A-3,

$$m = \frac{m_0}{f'} \qquad \text{(A-6a)}$$

$$h = \frac{h_0}{f'} \qquad \text{(A-6b)}$$

where

$$f' = \frac{f}{f_0} \qquad \text{(A-6c)}$$

Substitution of equations A-6 into equations A-4 and A-5 then gives

$$\frac{\mu_{eff}}{(\mu_{eff})_0} = 1 - \left[\frac{1}{(\mu_{eff})_0} - 1\right]\left[\frac{1 - (f')^2}{(f')^2 - h_0(m_0 + h_0)}\right] \qquad \text{(A-7a)}$$

$$\frac{\left(\frac{k}{\mu}\right)}{\left(\frac{k}{\mu}\right)_0} = \frac{f'\left[1 - h_0(m_0 + h_0)\right]}{(f')^2 - h_0(m_0 + h_0)} \qquad \text{(A-7b)}$$

Equation 6 of reference 1 still holds for the variation of parameter x,

$$\frac{x}{x_0} = f' \sqrt{\frac{\mu_{eff}}{(\mu_{eff})_0}} \qquad \text{(A-8a)}$$

Finally, the variation of parameter y is

$$\frac{y}{y_0} = \frac{\frac{1}{x}\left(\frac{k}{\mu}\right)}{\frac{1}{x_0}\left(\frac{k}{\mu}\right)_0} = \frac{1}{\sqrt{\frac{\mu_{eff}}{(\mu_{eff})_0}}} \left[\frac{1 - h_0(m_0 + h_0)}{(f')^2 - h_0(m_0 + h_0)}\right] \qquad \text{(A-8b)}$$

Note that equations A-4, A-5, A-7a, and A-8b reduce to the earlier expressions in references 1 and 4 upon the substitution of $h_0 = 0$.

To consider the sign of μ_{eff}, it is convenient to rewrite equation A-4 after substituting equations A-6,

$$\mu_{eff} = 1 - \frac{m_0(m_0 + h_0)}{(f')^2 - h_0(m_0 + h_0)} \qquad \text{(A-9)}$$

It can be seen that $\mu_{eff} < 0$ over the range

$$\sqrt{h_0(m_0 + h_0)} < f' < m_0 + h_0$$

APPENDIX B

MODIFICATION OF CIRCULATOR EQUATIONS FOR $\mu_{eff} < 0$

It is desired to calculate the scattering matrix (equations 20 to 24 of reference 4) of a circulator for the case of $\mu_{eff} < 0$. Thus, it is necessary to consider the effect of $\mu_{eff} < 0$ on equations 17 to 19 and hence equations 7 to 13 of reference 4 plus the relation (reference 3) $Z_{eff} = Z_0 \sqrt{\mu_{eff}/\epsilon}$. Denote by primes the values of parameters when $\mu_{eff} < 0$, and compare with the previous values for the same $|\mu_{eff}|$ and k/μ [k/μ in equation A-5 will remain negative for $f' > \sqrt{h_0(m_0 + h_0)}$],

$$x' = jx \tag{B-1a}$$

$$y' = -jy \tag{B-1b}$$

$$Z'_{eff} = jZ_{eff} \tag{B-1c}$$

Next, use is made of the relation (equation 13, Section 3.24 of reference 7) between Bessel functions of real and imaginary variables,

$$I_n(v) = j^{-n} J_n(jv) \tag{B-2}$$

Thus,

$$\frac{J_{n-1}(x')}{J_n(x')} = -j \frac{I_{n-1}(x)}{I_n(x)} \tag{B-3a}$$

$$A_n(x') = -j A_n(x), \text{ with I's instead of J's} \tag{B-3b}$$

Finally,

$$\left.\begin{aligned} L_0' &= L_0 \\ L_n' &= -L_n,\ n \neq 0 \\ K_n' &= -K_n \end{aligned}\right\} \text{ with I's instead of J's} \qquad \begin{aligned} &\text{(B-4a)} \\ &\text{(B-4b)} \\ &\text{(B-4c)} \end{aligned}$$

APPENDIX C

EFFECT OF IMPERFECT SYMMETRICAL MATCHING OF THREE-PORT CIRCULATOR

A lossless cyclic three-port circulator that is nonideal can be made ideal (Appendix I, paragraph B of reference 1) by inserting at each port identical lossless matching networks having input reflection coefficients

$$\rho_o = \frac{S_{12}}{S_{11}S_{12} - S_{13}^2} \tag{C-1}$$

In practice, a matching network can be designed only approximately to satisfy equation C-1 over a band of frequencies. Then, it is of interest to calculate the degradation in circulator performance, if the actual terminal reflection coefficients are

$$\rho = \rho_o + \delta, \quad |\delta| << |\rho_o| = \left|\frac{S_{12}}{S_{13}}\right| \tag{C-2}$$

First, consider the reverse gain to an isolated output port for a circulator that circulates from ports 1 to 2 to 3 to 1. From equation I-2 of reference 1, this gain is

$$G'_{31} = \left[1 - |\rho|^2\right]^2 \left|\frac{A_{13}}{\rho|E - PS|}\right|^2 \tag{C-3}$$

From Appendix I of reference 1 and equations C-1 and C-2 of this section, the component factors of equation C-3 are

$$\left[1 - |\rho|^2\right] = 1 - \left|\frac{S_{12}}{S_{13}}\right|^2 \left|1 - \frac{\delta\left(S_{13}^2 - S_{11}S_{12}\right)}{S_{12}}\right|^2 \qquad \text{(C-4)}$$

$$\left|\frac{A_{13}}{\rho}\right| = |\delta||S_{13}| \qquad \text{(C-5)}$$

and (after some manipulation)

$$||E - PS|| = |S_{13}|\left[1 - \left|\frac{S_{12}}{S_{13}}\right|^2\right]^2 \left|\left[1 + \frac{\delta\left(S_{12}^2 - S_{11}S_{13}\right)\left(S_{13}^3 - S_{11}S_{12}\right)}{S_{13}^3 - S_{12}^3}\right]^3 - \left[\frac{\delta\left(S_{13}^2 - S_{11}S_{12}\right)^2}{S_{13}^3 - S_{12}^3}\right]^3\right| \qquad \text{(C-6)}$$

Thus,

$$G'_{31} = \left\{\frac{|\delta|\left[1 - \left|\frac{S_{12}}{S_{13}}\right|^2 \left|1 - \frac{\delta\left(S_{13}^2 - S_{11}S_{12}\right)}{S_{12}}\right|^2\right]}{\left[1 - \left|\frac{S_{12}}{S_{13}}\right|^2\right]^2 \left|\left[1 + \frac{\delta\left(S_{12}^2 - S_{11}S_{13}\right)\left(S_{13}^2 - S_{11}S_{12}\right)}{S_{13}^3 - S_{12}^3}\right]^3 - \left[\frac{\delta\left(S_{13}^2 - S_{11}S_{12}\right)^2}{S_{13}^3 - S_{12}^3}\right]^3\right|}\right\}^2 \qquad \text{(C-7a)}$$

$$\approx \left[\frac{|\delta|}{1 - \left|\frac{S_{12}}{S_{13}}\right|^2}\right]^2, \quad |\delta| \ll \left|\frac{S_{12}}{S_{13}}\right| \qquad \text{(C-7b)}$$

Next, consider the forward gain to a normal output port of the same circulator. Similarly, this gain is

$$G'_{21} = \left[1 - |\rho|^2\right]^2 \left|\frac{A_{12}}{\rho|E - PS|}\right|^2 \qquad \text{(C-8)}$$

The only new factor appearing in equation C-8 is

$$\left|\frac{A_{12}}{\rho}\right| = |S_{13}| \left[1 - \left|\frac{S_{12}}{S_{13}}\right|^2\right] \left| 1 + \frac{\delta\left(S_{12}^2 - S_{11}S_{13}\right)\left(S_{13}^2 - S_{11}S_{12}\right)}{S_{13}^3 - S_{12}^3}\right| \qquad \text{(C-9)}$$

Thus,

$$G'_{21} = \left\{\frac{\left|1 + \frac{\delta\left(S_{12}^2 - S_{11}S_{13}\right)\left(S_{13}^2 - S_{11}S_{12}\right)}{S_{13}^3 - S_{12}^3}\right| \left[1 - \left|\frac{S_{12}}{S_{13}}\right|^2\right] \left|1 - \frac{\delta\left(S_{13}^2 - S_{11}S_{12}\right)}{S_{12}}\right|^2}{\left[1 - \left|\frac{S_{12}}{S_{13}}\right|^2\right] \left|\left[1 + \frac{\delta\left(S_{12}^2 - S_{11}S_{13}\right)\left(S_{13}^2 - S_{11}S_{12}\right)}{S_{13}^3 - S_{12}^3}\right]^3 - \left[\frac{\delta\left(S_{13}^2 - S_{11}S_{12}\right)}{S_{13}^3 - S_{12}^3}\right]^3\right|}\right\}^2 \qquad \text{(C-10a)}$$

$$\approx \left\{\frac{1 - \left|\frac{S_{12}}{S_{13}}\right|^2 \left|1 - \frac{\delta\left(S_{13}^2 - S_{11}S_{12}\right)}{S_{12}}\right|^2}{\left[1 - \left|\frac{S_{12}}{S_{13}}\right|^2\right] \left|1 + \frac{\delta\left(S_{12}^2 - S_{11}S_{13}\right)\left(S_{13}^2 - S_{11}S_{12}\right)}{S_{13}^3 - S_{12}^3}\right|^2}\right\}^2, \quad |\delta| \ll 1 \qquad \text{(C-10b)}$$

Examination of equation C-10b shows that the approximate forward gain G'_{21} of the imperfectly matched circulator depends not only on $|\delta|$ and $|S_{12}|/|S_{13}|$, but depends also on the phase

angles of the various quantities. It can be shown from the relations in Appendix I of reference 1, however, that the phase angles of the complex quantities.

$$\frac{\delta\left(S_{13}^2 - S_{11}S_{12}\right)}{S_{12}}$$

and

$$\frac{\delta\left(S_{12}^2 - S_{11}S_{13}\right)\left(S_{13}^2 - S_{11}S_{12}\right)}{S_{13}^3 - S_{12}^3}$$

are equal. Furthermore, it can be shown that the maximum value of forward gain occurs when these phase angles equal 0 and the minimum value when they equal π. Thus, the possible extreme values of forward gain are

$$\left|G'_{21}\right|_{max} \approx \left\{1 - \frac{1}{\left[\frac{1 - \left|\frac{S_{12}}{S_{13}}\right|^2}{|\delta|} + \left|\frac{S_{12}}{S_{13}}\right|\right]^2}\right\}^2$$

$$\approx 1 - \frac{2}{\left[\frac{1 - \left|\frac{S_{12}}{S_{13}}\right|^2}{|\delta|} + \left|\frac{S_{12}}{S_{13}}\right|\right]^2} \qquad \text{(C-11a)}$$

$$(G'_{21})_{min} \approx \left\{ 1 - \frac{1}{\left[\frac{1 - \left|\frac{S_{12}}{S_{13}}\right|^2}{|\delta|} - \left|\frac{S_{12}}{S_{13}}\right| \right]^2} \right\}^2$$

$$\approx 1 - \frac{2}{\left[\frac{1 - \left|\frac{S_{12}}{S_{13}}\right|^2}{|\delta|} - \left|\frac{S_{12}}{S_{13}}\right| \right]^2} \qquad \text{(C-11b)}$$

Last, consider the reflected power gain at a port of this circulator, which by conservation of power is

$$G'_{11} = 1 - \left| G'_{21} + G'_{31} \right| \qquad \text{(C-12)}$$

From equations C-7b, C-11, and C-12 the approximate possible extreme values of G'_{11} are

$$(G'_{11})_{max} \approx \left[\frac{|\delta|}{1 - \left|\frac{S_{12}}{S_{13}}\right|^2} \right]^2 \left\{ \frac{2}{\left[1 - \frac{|\delta| \left|\frac{S_{12}}{S_{13}}\right|}{1 - \left|\frac{S_{12}}{S_{13}}\right|^2} \right]^2} - 1 \right\}$$

$$\approx \left\{ \left[\frac{|\delta|}{1 - \left|\frac{S_{12}}{S_{13}}\right|^2} \right] \left[1 + \frac{2|\delta| \left|\frac{S_{12}}{S_{13}}\right|}{1 - \left|\frac{S_{12}}{S_{13}}\right|^2} \right] \right\}^2 \qquad \text{(C-13a)}$$

$$(G'_{11})_{min} \approx \left[\frac{|\delta|}{1 - \left|\frac{S_{12}}{S_{13}}\right|^2}\right]^2 \left\{\frac{2}{\left[1 + \frac{|\delta|\left|\frac{S_{12}}{S_{13}}\right|}{1 - \left|\frac{S_{12}}{S_{13}}\right|^2}\right]^2} - 1\right\}$$

$$\approx \left\{\left[\frac{|\delta|}{1 - \left|\frac{S_{12}}{S_{13}}\right|^2}\right]\left[1 - \frac{2|\delta|\left|\frac{S_{12}}{S_{13}}\right|}{1 - \left|\frac{S_{12}}{S_{13}}\right|^2}\right]\right\}^2 \qquad \text{(C-13b)}$$

Furthermore, the corresponding approximate extreme values of input SWR are

$$(SWR)_{max} = \frac{1 + \sqrt{(G'_{11})_{max}}}{1 - \sqrt{(G'_{11})_{max}}}$$

$$\approx \frac{1 + \left[\frac{|\delta|}{1 - \left|\frac{S_{12}}{S_{13}}\right|^2}\right]\left[1 + \frac{2|\delta|\left|\frac{S_{12}}{S_{13}}\right|}{1 - \left|\frac{S_{12}}{S_{13}}\right|^2}\right]}{1 - \left[\frac{|\delta|}{1 - \left|\frac{S_{12}}{S_{13}}\right|^2}\right]\left[1 + \frac{2|\delta|\left|\frac{S_{12}}{S_{13}}\right|}{1 - \left|\frac{S_{12}}{S_{13}}\right|^2}\right]} \qquad \text{(C-14a)}$$

$$(\mathrm{SWR})_{\min} = \frac{1 + \sqrt{(G'_{11})_{\min}}}{1 - \sqrt{(G'_{11})_{\min}}}$$

$$\approx \frac{1 + \left[\dfrac{|\delta|}{1 - \left|\dfrac{S_{12}}{S_{13}}\right|^2}\right]\left[1 - \dfrac{2|\delta|\left|\dfrac{S_{12}}{S_{13}}\right|}{1 - \left|\dfrac{S_{12}}{S_{13}}\right|^2}\right]}{1 - \left[\dfrac{|\delta|}{1 - \left|\dfrac{S_{12}}{S_{13}}\right|^2}\right]\left[1 - \dfrac{2|\delta|\left|\dfrac{S_{12}}{S_{13}}\right|}{1 - \left|\dfrac{S_{12}}{S_{13}}\right|^2}\right]} \qquad \text{(C-14b)}$$

APPENDIX D
ANALYSIS OF TWO-SECTION QUARTER-WAVELENGTH TRANSFORMER FOR MATCHING CIRCULATOR

Figure D-1 shows the equivalent circuit of a two-section quarter-wavelength transformer for matching each port of a three-port strip-transmission-line circulator. The strip transmission line between the transformer and the terminals of the circulator has a characteristic impedance Z_0 equal to the load impedance. The characteristic impedances of each section of the transformer (Z_1 and Z_2) are chosen such that $Z_2 < Z_1 < Z_0$, and the equal electrical lengths of each section (θ) are chosen to be a quarter-wavelength at the desired center frequency. It is desired to calculate the input reflection coefficient referred to a Z_0-line and to investigate the effect of varying the impedance ratios Z_1/Z_0 and Z_2/Z_0.

By straightforward calculations, the over-all ABCD matrix of the circuit of Figure D-1 is

$$\begin{bmatrix} A & B \\ C & D \end{bmatrix} = \begin{bmatrix} \cos^2\theta - \frac{Z_2}{Z_1}\sin^2\theta & j(Z_1 + Z_2)\sin\theta\cos\theta \\ j\left(\frac{1}{Z_1} + \frac{1}{Z_2}\right)\sin\theta\cos\theta & \cos^2\theta - \frac{Z_1}{Z_2}\sin^2\theta \end{bmatrix} \quad \text{(D-1)}$$

Thus, the input reflection coefficient referred to Z_0 is

$$\rho = \frac{A + \frac{B}{Z_0} - \left(CZ_0 + D\right)}{A + \frac{B}{Z_0} + CZ_0 + D}$$

$$= \frac{s_0^{1/2} - s_0^{-1/2} - j\left(s_0^{1/4} + s_0^{-1/4}\right)\left(s_1^{1/2} - s_1^{-1/2}\right)\cot\theta}{2\cot^2\theta - \left(s_0^{1/2} + s_0^{-1/2}\right) + j\left(s_0^{1/4} + s_0^{-1/4}\right)\left(s_1^{1/2} + s_1^{-1/2}\right)\cot\theta} \qquad \text{(D-2a)}$$

where

$$s_0 = \left(\frac{Z_1}{Z_2}\right)^2 > 1 \qquad \text{(D-2b)}$$

$$s_1 = \frac{Z_0^2}{Z_1 Z_2} > 1 \qquad \text{(D-2c)}$$

Examination of equation D-2a shows that the locus of ρ versus θ is symmetrical about the real ρ-axis for values of θ having arithmetic symmetry about $\pi/2$ (or, alternatively, values of frequency having arithmetic symmetry about the center frequency). Furthermore, at $\theta = \pi/2$, $\rho = -(s_0 - 1)/(s_0 + 1)$, which on a Smith chart is the point $R/Z_0 = 1/s_0$ (SWR = s_0) and $X/Z_0 = 0$. Concerning the remainder of the locus, it can be shown that if $(Z_1/Z_0)^3 = Z_2/Z_0$, or $s_1 = s_0$, the transformer is the usual maximally flat amplitude design. The resulting locus (Figure D-2) is heart-shaped with a cusp at the above mentioned point on a Smith chart and passes through the point $R/Z_0 = 1$, $X/Z_0 = 0$ (the origin of the ρ-plane) at $\theta = 0$ or π.

It is also of interest to consider what happens if $s_1 > s_0$. Then, it can be shown that the locus makes a small loop (Figure D-2) to intersect the real ρ-axis at $\rho = -(s_1 - 1)/(s_1 + 1)$, which on a Smith chart is the point $R/Z_0 = 1/s_1$ (SWR = s_1) and $X/Z_0 = 0$.

The corresponding value of θ is

$$\theta = \cot^{-1}\left[\frac{s_1 - s_0}{s_0^{1/2}(s_1 - 1)}\right]^{1/2} \qquad \text{(D-3)}$$

For design purposes, if values of s_0 and s_1 are specified to give a desired locus, from equations D-2b and D-2c the appropriate values of normalized line impedances are

$$\frac{Z_1}{Z_0} = \frac{s_0^{1/4}}{s_1^{1/2}} \qquad \text{(D-4a)}$$

$$\frac{Z_2}{Z_0} = \frac{1}{s_0^{1/4}\, s_1^{1/2}} \qquad \text{(D-4b)}$$

In particular, if these line impedances are obtained by using dielectric rings with a Z_0-line, the appropriate values of dielectric constant are, respectively,

$$\epsilon_1 = \frac{s_1}{s_0^{1/2}} \qquad \text{(D-5a)}$$

$$\epsilon_2 = s_1 s_0^{1/2} \qquad \text{(D-5b)}$$

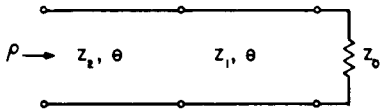

FIGURE D-1. EQUIVALENT CIRCUIT OF TWO-SECTION QUARTER-WAVELENGTH TRANSFORMER FOR MATCHING CIRCULATOR

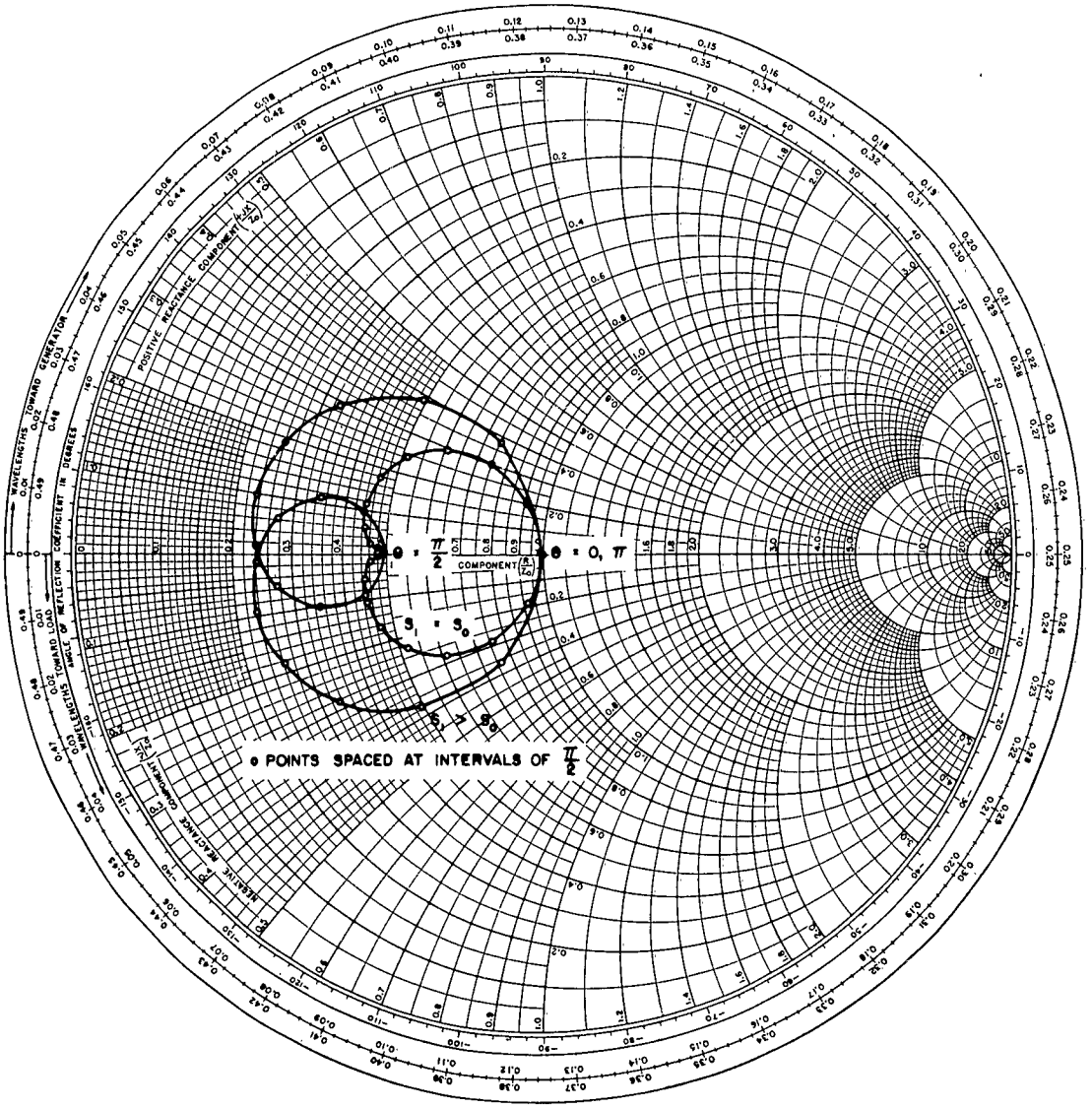

FIGURE D-2. LOCUS OF REFLECTION COEFFICIENT OF TWO-SECTION QUARTER-WAVELENGTH TRANSFORMER FOR MATCHING CIRCULATOR

APPENDIX E
DERIVATION OF BALANCED AMPLIFIER INPUT IMPEDANCE

The equivalent circuit used to derive the input impedance of the balanced amplifier is shown in Figure E-1, where use was made of a Hyltin unpumped-diode equivalent circuit (reference 8) shown in Figure E-2. In these circuits C_s and C_a are the stray capacitances in the diode lead inductance, R_D is the diode series resistance, C_o is the static junction capacitance, and C_b consists of C_s and one half the strays contributed by the diode holder. The derivation is based upon analyzing only one of the balanced diodes; consequently, the final result will be equal to one half of the derived expression. In addition, ideal transformers and circulators are assumed.

The time varying capacitance is represented by augmenting the matrix introduced by Matthaei (reference 9), with the diode series resistance R_D; this yields:

$$Z = \begin{pmatrix} Z_{11} & Z_{12} \\ Z_{21} & Z_{22} \end{pmatrix} = \begin{pmatrix} R_D - jX_{11} & jX_{12} \\ jX_{21} & R_D + jX_{22} \end{pmatrix} \qquad \text{(E-1)}$$

where

$$X_{11} = \frac{1}{j\omega_1 C_o(1 - a^2)}$$

$$X_{22} = \frac{1}{-j\omega_1 C_o(1 - a^2)}$$

$$X_{12} = \frac{1}{j\omega_1 C_o(1 - a^2)}$$

$$X_{21} = \frac{1}{-j\omega_2 C_o(1 - a^2)}$$

The input impedance at reference plane T of Figure E-2 (assuming that all the higher order harmonics are short circuited), is then given by:

$$Z_T = Z_{11} - \frac{Z_{12}\, Z_{21}}{Z_2^* + Z_{22}} = R_D' + jX' \qquad \text{(E-2)}$$

where Z_2^* = conjugate of the idler load. Once Z_2^* is known, Z_T can be found. In the balanced amplifier used in the experiments, the idler load is a parallel resonant circuit consisting of the diode lead inductance and the internal strays of one of the diodes. Thus,

$$R_D' = R_D\left[1 - \frac{X_{12}\, X_{21}}{R_D^2 + \left(X_{22} - \frac{\omega_2 L}{\omega_2 C_a - 1}\right)^2}\right] \qquad \text{(E-3a)}$$

$$X' = \left[\frac{X_{12}\, X_{21}\left(X_{22} - \frac{\omega_2 L}{X_{22}\omega_2 C_a - 1}\right)}{R_D^2 + \left(X_{22} - \frac{\omega_2 L}{\omega_2 C_a - 1}\right)^2} - X_{11}\right] \qquad \text{(E-3b)}$$

Equations E-3a and E-3b are readily transformed to obtain the input impedance at reference plane "a."

$$z_{in} = \frac{R_D' + j\left\{R_D'^2\left[1 - \omega_1^2 C_a L\right]\left[\omega_1 C_a + \omega_1 C_b\left[1 - \omega_1^2 C_a L\right]\right] - \left[X' + \omega_1 L\left[1 - \omega_1 C_a X'\right]\right]\left[\left(1 - \omega_1 C_a X'\right)\left(1 - \omega_1^2 C_b L\right) - \omega_1 C_b X'\right]\right\}}{\left[\left(1 - \omega_1 C_a X'\right)\left(1 - \omega_1^2 C_b L\right) - \omega_1 C_b X'\right]^2 + \left(R_D' \omega_1 C_a\right)^2\left[1 + \frac{C_b}{C_a}\left(1 - \omega_1^2 C_a L\right)\right]^2} \qquad (E-4)$$

Equation E-4 is in the process of being programmed for a Recomp II digital computer. The results will be presented in the next report period.

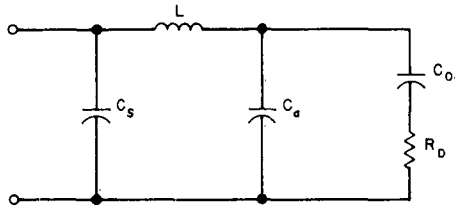

FIGURE E-1. EQUIVALENT CIRCUIT OF UMPUMPED VARACTOR

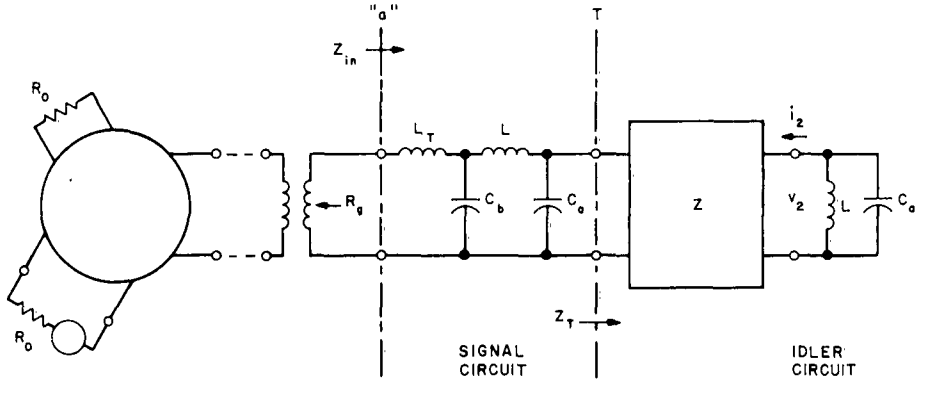

FIGURE E-2. EQUIVALENT CIRCUIT OF AMPLIFIER

DISTRIBUTION LIST FOR REPORT NO. 1654-I-3

Copy No.	Address	No. of Copies
1 thru 3	**RADC (RALTM, ATTN: Lt. Becker) Griffiss AFB, New York	3
4	*RADC (RAAPT) Griffiss AFB, New York	1
5	*RADC (RAALD) Griffiss AFB, New York	1
6	*GEEIA (ROZMCAT) Griffiss AFB, New York	1
7	*RADC (RAIS, ATTN: Mr. Malloy) Griffiss AFB, New York	1
8	*U.S. Army Electronics R&D Labs Liaison Officer RADC Griffiss AFB, New York	1
9	*AUL (3T) Maxwell AFB, Alabama	1
10	ASD (ASAPRD) Wright-Patterson AFB, Ohio	1
11	Chief, Naval Research Lab ATTN: Code 2027 Wash 25, D. C.	1
12	Air Force Field Representative Naval Research Lab ATTN: Code 1010 Wash 25, D. C.	1
13	Commanding Officer U.S. Army Electronics R&D Labs ATTN: SELRA/SL-ADT Ft Monmouth, New Jersey	1
14	National Aeronautics & Space Admin Langley Research Center Langley Station Hampton, Virginia ATTN: Librarian	1

DISTRIBUTION LIST FOR REPORT NO. 1654-I-3 (cont)

Copy No.	Address	No. of Copies
15	AFSC (SCSE) Andrews AFB Wash 25, D. C.	1
16	Commanding General U.S. Army Electronics Proving Ground ATTN: Technical Documents Library Ft Huachuca, Arizona	1
17 thru 26	*ASTIA (TISIA-2) Arlington Hall Station Arlington 12, Virginia	minimum of 10
27	AFSC (SCFRE) Andrews AFB Wash 25, D. C.	1
28	Commander U.S. Naval Air Dev Cen (NADC Lib) Johnsville, Pennsylvania	1
29	Director U.S. Army Engineer R&D Labs Technical Documents Center Ft Belvoir, Virginia	1
30	ESD (ESRL) LG Hanscom Field Bedford, Massachusetts	1
31	Commanding Officer & Director U.S. Navy Electronics Lab (LIB) San Diego 52, California	1
32	ESD (ESAT) LG Hanscom Field Bedford, Massachusetts	1
33	RADC (RAWED/Mr. Friedman) Griffiss AFB, New York	1
34 and 35	Advisory Group on Electronic Devices ATTN: Mr. Warren Kramer 346 Broadway New York 13, New York	2
36	Federal Scientific Corp. 615 West 131st Street New York 27, New York	1
37	Microwave Associates ATTN: Dr. L. Gould Burlington, Massachusetts	1

DISTRIBUTION LIST FOR REPORT NO. 1654-I-3 (cont)

Copy No.	Address	No. of Copies
38	Sperry Microwave Electronics Co. ATTN: Mr. B. Duncan Clearwater, Florida	1
39	SFD Laboratories, Inc. ATTN: Dr. J. Saloom 808 Rahway Avenue Union, New Jersey	1
40	Hughes Aircraft Co. Hughes Research Labs Culver City, California	1
41	Chief, Bureau of Ships ATTN: Code 312 Main Navy Bldg Wash 25, D. C.	1
42	Office of the Chief Signal Officer Department of the Army ATTN: SIGRD Wash 25, D. C.	1
43	AFPRO General Electric Co. Lockland Br. PO Box 91 Cincinnati 15, Ohio	1

** Project Engineer will enter his office symbol and name in space provided.

* Mandatory.